Planar Coulomb bicrystals

I. M. Buluta and S. Hasegawa
Department of Quantum Engineering and Systems Science, The University of Tokyo, 7-3-1, Hongo, Bunkyo-ku, Tokyo, 113-8656, Japan
(Received 30 June 2008; published 31 October 2008)

We numerically studied two-component planar Coulomb crystals (planar bicrystals) in rf traps. The number of ions in the inner shell was found to be limited by the mass difference between the two components and we calculated the maximum possible number of ions in the inner shells for various mass ratios. When large axial potentials are applied the spatial separation between components depends on the trapping parameters as well as on the ion masses and charges. We derived the spatial separation both theoretically and numerically and discussed its effect on the efficiency of sympathetic cooling and on rf heating. We suggest using planar bicrystals for implementing quantum simulation and computation.

DOI: 10.1103/PhysRevA.78.042340 PACS number(s): 03.67.Lx, 02.70.Ns, 37.10.Ty

I. INTRODUCTION

Planar Coulomb crystals in ion traps are interesting examples of two-dimensional charged-particle systems, their study having relevance for electrons in quantum dots [1], electrons on the surface of liquid helium [2], dusty plasmas [3], or confined ferromagnetic particles [4]. Moreover, planar Coulomb crystals have recently come into attention due to the quantum simulation and computation scheme proposed in [5,6]. Quantum simulation with planar Coulomb crystals looks very promising and there are already several suggested applications such as: effective quantum spin models [7,8], Bose-Einstein condensation [9], or spin-boson models [10]. Furthermore, planar crystals offer the prospect of realizing large-scale ion-trap quantum computation and even measurement-based quantum computation [11].

Planar crystals in ion traps have been studied theoretically [12] and small crystals (up to 19 ions) have been experimentally realized [13], but so far they remained no more than a curiosity. Multicomponent charged particles trapped in a two-dimensional quadratic trap have been considered in [14,15] but the particular features of ion traps such as the mass separation have not been taken into consideration. In [16] we analyzed one-component planar Coulomb crystals in detail. In this paper we discuss two- and multicomponent planar crystals (either different elements or isotopes of the same element). We will refer to two-component planar crystals as planar bicrystals. Since the results on planar bicrystals can be easily extended to the multicomponent case in the following discussion we will generally consider bicrystals. Bicrystals have been known for some time and there are several experimental and theoretical studies that have investigated their properties [17–19]. However, to the best of our knowledge there are no results on planar bicrystals in rf traps. Our motivation for studying planar bicrystals is twofold. On one hand we wish to investigate the properties of planar bicrystals which are particularly interesting from a theoretical point of view and relevant for several other physical systems. Due to the anisotropic confinement planar crystals behave very differently from the three-dimensional ones [12]. Moreover, when two or more species of ions are involved, new features, such as mass separation, for example, are expected to emerge. On the other hand we envisage using them for quantum simulation and computation by exploiting sympathetic cooling.

The paper is structured as follows: first, we review previous theoretical and experimental results on bicrystals and planar crystals and describe our simulation methods. In Sec. IV, we present our results on the structure of planar bicrystals and the spatial separation. Next, we discuss sympathetic cooling and rf heating. Finally, we consider the possibility of implementing quantum simulation and computation with planar bicrystals, make a few comments on the experimental issues, and then draw the conclusions.

II. BACKGROUND

Trapped, cooled ions crystallize when the coupling parameter $\Gamma > 170$, $\Gamma = Q^2/a_{WS}k_BT$, where a_{WS} is the Wigner-Seitz radius $[(4\pi/3)n_0a_{WS}=1$, n_0 the particle number density] and T is the temperature. In the case of infinite plasmas bcc crystals are expected. However, in experiments the number of ions is not large enough and the crystal structure is determined by the boundary conditions set by the confining potentials. One-dimensional (1D), 2D, and 3D structures varying from strings and zigzags to spheroidal crystals have been observed in experiments (see [20], Chap. 18). Planar crystals are quite special due to the anisotropic confinement [12]. Because of this the ion density is not constant [21] and therefore it is not possible to define Γ. Moreover, due to the nonuniform density, particular features are expected to emerge, especially in the rf-heating behavior [16]. The shape of Coulomb crystals depends on the confining potentials (see [12,20,21]). It can be described in using the anisotropy parameter which is the ratio between the axial and radial frequencies, $\alpha = \omega_z^2/\omega_{xy}^2$. An oblate spheroidal crystal with N ions will turn into a planar one when the anisotropy parameter, α is larger than the threshold $\alpha_3(N)$.

$$\alpha > \alpha_3(N) = \left(\frac{96N}{\pi^3 w_1^3}\right)^{1/2}, \tag{1}$$

where $w_1 = 1.11\ldots$ [20,22]. Since our interest lies especially in Coulomb crystals in linear rf traps where the confining potentials near the trap center can be well-approximated as harmonic, the above theoretical results will be our starting point.

In a linear rf trap, because the radial confining potential is mass dependent while the axial confining potential is not, a spatial separation leading to complex shell structures occurs. Lighter ions gather close to the trap axis while the heavier ones surround them forming a second shell [17,19]. Assuming that the ions' masses are $M_1 < M_2$ and the charges are Q_1 and Q_2, respectively, the ratio of the outer radius of the inner shell, b_1, and the inner radius of the outer shell a_2, is proportional to the square root of the ratio of the masses, $b_1/a_2 = (Q_2/Q_1)(M_1/M_2)^{1/2}$ [23,17]. As mentioned before, the structure of the ground state of multicomponent charged particles confined in a 2D trap has been investigated in [14,15]. However, these studies do not consider the spatial separation due to the mass dependence of the trapping frequencies. Because of this the shells' composition and separation are different: the particles having the largest mass-to-charge ratio are located nearest to the center. As for ions with identical charge-to-mass ratios it was shown that, after cooling, the crystallized state consists of a mixed core surrounded by nearly degenerated double shells of the different species [18].

III. SIMULATION

We used molecular dynamics simulations to study planar bicrystals. Our simulations are designed using the ProtoMol framework [24], which has been already extensively tested for Coulomb crystals simulations (see, for example, [18,19]). The simulations ran on a Core2Duo 2.4 GHz 2 GB/RAM machine. The framework gives much flexibility in the programming by allowing the modeling of various forces. The simulation methods have been described in detail in [16]. In the static approximation, the axial potential for an ion of mass M_i and charge Q_i is

$$\Phi_z = \frac{1}{2} M_i \omega_z^2 z^2, \tag{2}$$

where ω_z is the axial confining frequency (for a linear segmented rf trap $\omega_z^2 = 2kQ_iU_z/M_iz_0^2$, where k is a geometric constant, U_z the voltage applied to the outer segments, and $2z_0$ is the length of the inner segment). The radial potential is

$$\Phi_r = \frac{1}{2} M_i \left(\omega_r^2 - \frac{1}{2}\omega_z^2 \right)(x^2 + y^2), \tag{3}$$

where ω_r is the radial confining frequency (for a linear segmented rf trap $\omega_r^2 = Q_i^2 U_{ac}^2 / 2M_i^2 r_0^4 \Omega^2$, where U_{ac} and Ω are the amplitude and frequency of the rf field and r_0 is the distance from the trap center to the surface of the electrodes). The time-dependent rf potential is

$$\Phi = U_{ac} \cos \Omega t \frac{x^2 - y^2}{2r_0^2} + \frac{kU_z}{z_0^2}\left(z^2 - \frac{(x^2 + y^2)}{2} \right). \tag{4}$$

Due to the presence of the axial voltage, the radial potential is shifted $\omega_{xy} = \sqrt{\omega_r^2 - \frac{1}{2}\omega_z^2}$ [25]. This has important consequences in the case of planar bicrystals as we will see in the following section.

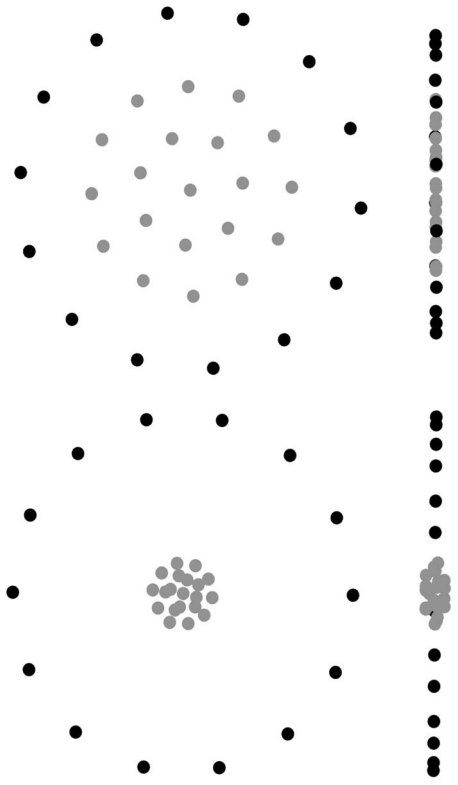

FIG. 1. (Upper) Planar bicrystal composed of 20 $^{40}Ca^+$ (gray) and 14 $^{44}Ca^+$ (black) ions, radius $\sim 40\ \mu$m, radial separation $\sim 16\ \mu$m. (Lower) Bicrystal composed of 20 $^{24}Mg^+$ (gray) and 14 $^{44}Ca^+$ (black) ions, radius $\sim 55\ \mu$m, radial separation $\sim 32\ \mu$m. Radial and axial plane views. The simulations are performed using static potential.

IV. RESULTS

A. Structure of planar bicrystals

In the following we will consider the ions being trapped in a linear segmented rf trap, whose radial and axial potentials have been described above. This approach is more meaningful than simply considering two arbitrary frequencies ω_{xy} and ω_z because it is directly relevant to the experiment. Note that the trap geometric and operating parameters can be adjusted in order to obtain the desired frequencies and the radial frequency shift is taken into consideration. Let us begin by taking a look at the anisotropy parameter, $\alpha = \omega_z^2/\omega_{xy}^2$, for various ion species as a function of the axial voltage U_z. As U_z increases, the anisotropy parameter increases faster for the heavier ions, therefore, in a bicrystal the outer shell will become planar before the inner one. This is illustrated in Fig. 1 by a perfectly planar bicrystal composed of 20 $^{40}Ca^+$ and 14 $^{44}Ca^+$ and a bicrystal (not planar) composed of 20 $^{24}Mg^+$ and 14 $^{44}Ca^+$. The radial confinement is much weaker for the $^{24}Mg^+ - ^{44}Ca^+$ bicrystal ($\alpha = 1.2$) than for the $^{40}Ca^+ - ^{44}Ca^+$ one ($\alpha = 9.3$) because otherwise the ions would be forced out of the trap. In the case of the $^{24}Mg^+ - ^{44}Ca^+$ bicrystal no matter how we adjust the trapping parameters (i.e., increase α) it will not become perfectly planar. The anisotropy parameter reaches its maximum when

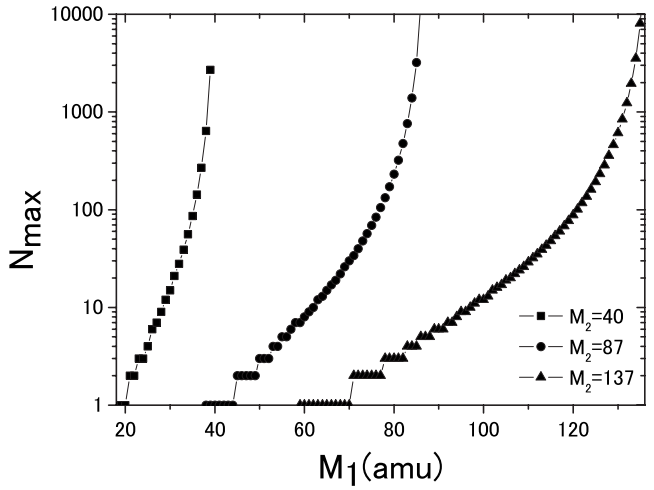

FIG. 2. N_{max} as a function of the mass of the light ions for different values of M_2. $M_2=40$ (square), $M_2=87$ (dot), and $M_2=137$ (triangle).

$\omega_r^2-\frac{1}{2}\omega_z^2$ is very small (i.e., $Q_iU_{ac}^2z_0^2-2kU_zM_ir_0^4\Omega^2$ is very small). As $Q_iU_{ac}^2z_0^2-2kU_zM_ir_0^4\Omega^2\leqslant 0$ the ions of type i cannot be trapped anymore because they are forced out of the trap by the axial potential which is stronger than the radial one. It follows that there exists a certain maximum number of light ions such that both shells are planar. This number, N_{max}, does not depend on the trapping parameters. Considering a bicrystal with ions of masses $M_1<M_2$, $(Q_1=Q_2)$ N_{max} can be easily derived from the following equation:

$$\alpha_3(N_{max})=\frac{2M_1}{M_2-M_1}. \tag{5}$$

If the charges are not equal, then $\alpha_3(N_{max})=2Q_2M_1/(Q_1M_2-Q_2M_1)$. Note that for species with identical charge-to-mass ratio the anisotropy parameter is the same. This case is special and will be discussed later. Using the above equation, we can derive the maximum number of ions in the inner shell for perfectly planar bicrystals (i.e. both the inner and outer shell are planar). The results are shown in Fig. 2. We calculated N_{max} as a function of M_1 for different values of M_2. The charges are assumed to be equal. When the mass difference is large one can observe a stepwise behavior that disappears as the mass difference becomes smaller. Here are some examples of interest for experiments: $^{40}Ca^+-^{44}Ca^+$ $N_{max}=176$, $^{24}Mg^+-^{26}Mg^+$ $N_{max}=254$, $^{24}Mg^+-^{40}Ca^+$ $N_{max}=3$, $^{137}Ba^+-^{200}Hg^+$ $N_{max}=8$, and $^{87}Sr^+-^{137}Ba^+$ $N_{max}=5$. It follows that perfectly planar bicrystals with many light ions are not always possible, especially when the ions have very different masses. Consequently, planar bicrystals with a large inner shell are only possible for ions with a very small mass difference, for example, isotopes of the same element like $^{44}Ca^+-^{44}Ca^+$ or $^{24}Mg^+-^{26}Mg^+$.

In Fig. 3 four examples of planar bicrystals with different numbers and types of ions are shown. The values of α for the light ions are 3.7 (a), 9.3 (b) and (c), and 16 (d). In (a) and (b) the number of ions is identical but the ratio of masses is different so the effect of the spatial separation can be easily observed. A large separation between the components can be seen in (a) as compared to (b) where the mass difference being small, the separation is also small. In (c) the 20 $^{40}Ca^+$

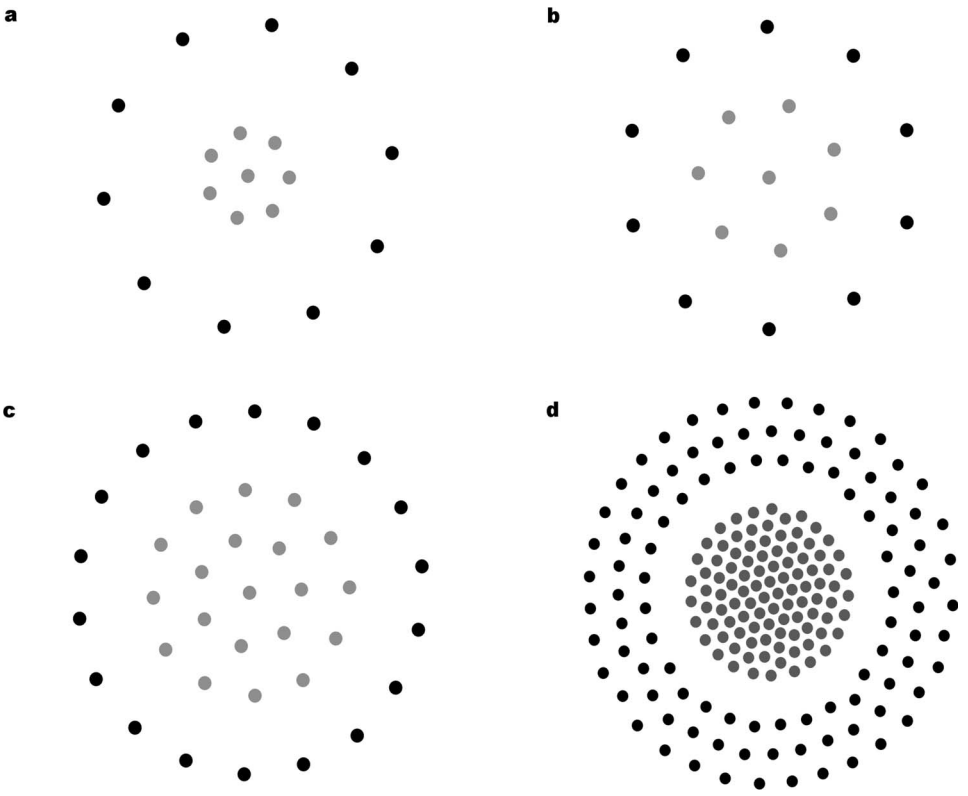

FIG. 3. Examples of planar bicrystals (not to scale). (a) eight $^{137}Ba^+$ (gray) and ten $^{200}Hg^+$ (black) ions, radius ~35 μm, (b) eight $^{24}Mg^+$ (gray) and ten $^{26}Mg^+$ (black) ions, radius ~33 μm, (c) 20 $^{40}Ca^+$ (gray) and 18 $^{44}Ca^+$ (black) ions, radius ~42 μm, and (d) 100 $^{40}Ca^+$ (gray) and 100 $^{44}Ca^+$ (black) ions, radius ~517 μm. The simulations are performed using static potential.

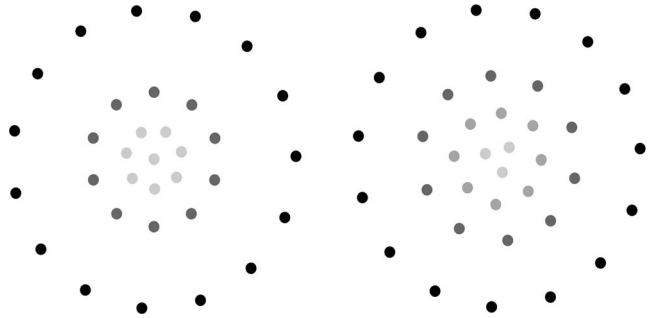

FIG. 4. (Left) Planar crystal containing three ion species: $m=44$ (black), $m=40$ (dark gray) and $m=34$ (light gray). The radius is ~ 75.7 μm. (Right) Planar crystal containing four ion species: $m=44$ (black), $m=40$ (dark gray), $m=38$ (gray) and $m=34$ (light gray). The radius is ~ 79 μm. The simulations are performed using static potential.

ions are completely surrounded by a ring of $^{44}Ca^{+}$ ions. The same thing happens in (d) where we can observe the $^{44}Ca^{+}$ ions forming three rings. For planar bicrystals the inner shell has the typical structure of a 2D Wigner crystal described in [26] while the outer shell always consists of well-defined concentric rings [see Fig. 3(d)]. The inner shell has the a nice triangular-lattice structure that would be useful for implementing quantum simulation and computation. In Fig. 4 two examples of multicomponent planar crystals are shown: a planar crystal containing three ion species: $m=44$, 40, and 34 and a planar crystal containing four ion species: $m=44$, 40, 38, and 34. For the former the radius is ~ 75.7 μm, while for the latter the radius is ~ 79 μm. The shell structure is very obvious here, too.

We also considered planar bicrystals with identical charge-to-mass ratio. In Fig. 5 an example of such a crystal containing 20 $^{40}Ca^{+}$ and 20 $^{80}Al^{2+}$ ions is shown. The radius is ~ 35 μm. In this case there are no shells and ions of different masses form a mixed core (see also [18]). The final configuration depends on the initial conditions. The distance between neighboring ions is variable because the Coulomb repulsion is different: the $^{40}Ca^{+}-^{80}Al^{2+}$ minimum distance is about 9 μm, the $^{40}Ca^{+}-^{40}Ca^{+}$ minimum distance is ~ 8 μm, and the $^{80}Al^{2+}-^{80}Al^{2+}$ minimum distance is ~ 10 μm. This special case is not of interest neither for our theoretical results concerning the spatial separation and the maximum number of ions in the inner shell nor for implementing quantum simulation and computation. However, it should be mentioned as an exceptional case.

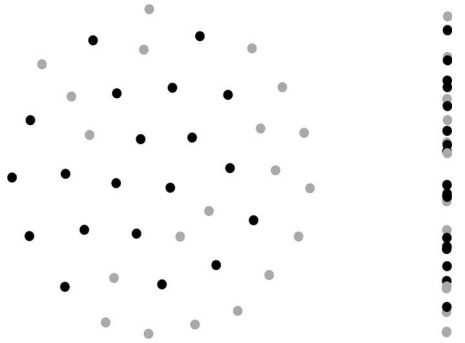

FIG. 5. Planar bicrystal with identical charge-to-mass ratio: 20 $^{40}Ca^{+}$ (gray) and 20 $^{80}Al^{2+}$ (black) ions. Radial and axial plane views. The radius is ~ 35 μm. The simulations are performed using static potential.

B. Spatial separation

For the isotopes of the same element, the spatial separation between shells is about the same as the average distance between the ions. This can be seen in Fig. 1 (upper). As predicted by theory, for planar bicrystals with a large mass difference between the two components, the spatial separation is also large. This is illustrated in Fig. 1 (lower). The spatial separation will influence the efficiency of sympathetic cooling as suggested in [17]. We mentioned in Sec. II that the spatial separation between ions depends only on the ion charges and masses. If we denote by b_i the outer radius of shell i (mass M_i) and by a_i the corresponding inner radius we get [23]

$$\frac{b_i}{a_{i+1}} = \frac{Q_{i+1}}{Q_i}\sqrt{\frac{M_i}{M_{i+1}}}. \tag{6}$$

We have $M_1 < M_2 < \cdots$ and of course $a_1 = 0$. It is obvious that the separation occurs because the pseudopontentials are unequal. If we do not consider the radial frequency shift due to the application of the static potential U_z (see Sec. III), the ratio of the outer and inner radii of the shells depends only on the ion charges and masses. However, when U_z is large (as in the case of planar bicrystals) we have to take into consideration the effect of the radial frequency shift. We derived the spatial separation theoretically like in [23,27] and obtained

$$\frac{b_i}{a_{i+1}} = \sqrt{\frac{Q_{i+1}^2 U_{ac}^2 z_0^2 - 2kU_z Q_{i+1} M_{i+1} r_0^4 \Omega^2}{Q_i^2 U_{ac}^2 z_0^2 - 2kU_z Q_i M_i r_0^4 \Omega^2}\frac{M_i}{M_{i+1}}}. \tag{7}$$

By taking $U_z = 0$ V we recover Eq. (6). In the limit of $M_i \simeq M_{i+1}$ and $Q_i = Q_{i+1}$, $b_i/a_{i+1} \simeq 1$ as expected. We compared the theoretical results given by Eq. (7) with the molecular dynamics simulations and we found them to be in good agreement. This is shown in Fig. 6. For the numerical values from the molecular dynamics simulations corrections were required due to the fact that the estimated b_i and a_{i+1} are not precisely the same as the theoretical ones. In the simulations when $M_i \simeq M_{i+1}$, b_i/a_{i+1} does not become 1. This is because there is always some distance between the ions so b_i is never quite equal to a_{i+1} as in the theory. Moreover, as $M_i \simeq M_{i+1}$ the components become mixed and instead of a shell structure we get something similar to the configuration in Fig. 5. The corrections were made such that the minimum distance between the ions is taken into consideration when calculating b_i and a_{i+1}.

V. DISCUSSION

A. Sympathetic cooling and rf heating

The idea of using sympathetic cooling in quantum computation is certainly not new [28,29]. Several studies have investigated sympathetic cooling using both molecular dy-

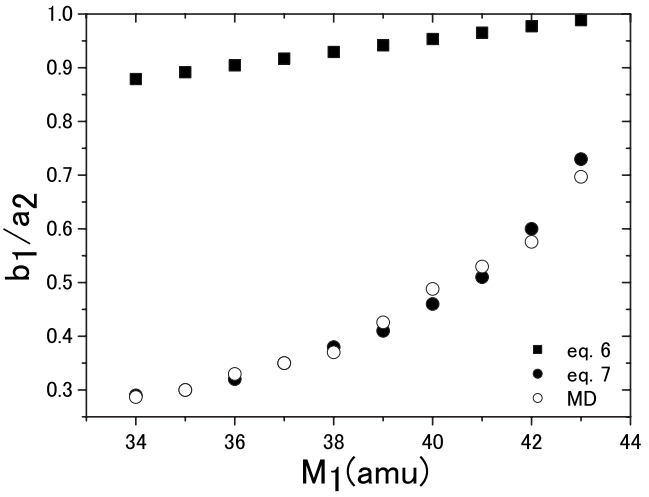

FIG. 6. The spatial separation b_1/a_2 as calculated from Eq. (7) (square), Eq. (6)(dot), and derived from molecular dynamics simulations (circle).

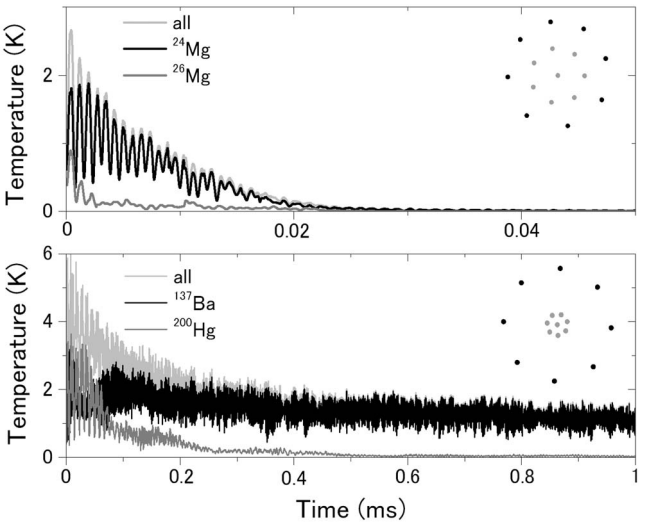

FIG. 7. (Upper) Sympathetic cooling of eight $^{24}Mg^+$ (gray) and eight $^{26}Mg^+$ (black). $^{26}Mg^+$ is directly cooled. The final temperatures are in the μK range. (Lower) Sympathetic cooling of eight $^{137}Ba^+$ (gray) and eight $^{200}Hg^+$ (black). $^{200}Hg^+$ is directly cooled. The final temperature for Ba is $\sim$1 K and for Hg$\sim$0.03 K. The insets show the respective bicrystals. The simulation is performed using static potential.

namics simulations and experimental data [30–32]. However, sympathetic cooling has not been considered before in the context of planar crystals. The reason why we are interested in the sympathetic cooling of planar bicrystals is that we wish to keep a planar crystal cold for a long time in order to be able to perform quantum simulation and computation. For this purpose continuously cooling the outer shell of a planar bicrystal would help maintain the inner shell at a low temperature, which in turn would allow us to use it for implementing quantum simulation and computation.

Let us first take a look at the theory of sympathetic cooling. It is well-known that the efficiency of sympathetic cooling depends on the number of ions and the spatial overlap between the two species [20]. The sympathetic cooling of ions in the gas phase has been investigated in [31]. However, in the crystal phase the efficiency of sympathetic cooling depends on the spatial separation as suggested in [17]. The trapping parameters also influence the sympathetic cooling rate because they determine the rf-heating rate (see [16]).

Figure 7 illustrates the effect of spatial separation on the efficiency of sympathetic cooling. Only here we used static potential such that rf heating does not affect the results. In both cases we used trapping potentials providing $\alpha \sim 5$ (for the light ions) and we directly cooled the heavy ions. We plotted the average temperatures of the light, the heavy and all the ions. The upper graph shows the sympathetic cooling of eight $^{24}Mg^+$ and eight $^{26}Mg^+$ (the crystal is shown in the inset). Since the separation is small the efficiency of sympathetic cooling is high. The temperature decreases very fast for both the directly and sympathetically cooled ions. The final temperatures are in the μK range. Note that in the simulation we can reach arbitrarily low temperatures (far lower than the Doppler limit). This is because heating mechanisms such as rf heating, heating due to "patch fluctuations" or the imperfections of the trap electrodes, and diffusive heating are not taken into consideration. The reason for this is that, except for the rf heating, these phenomena are rather difficult to model and quantify. In the lower graph (eight $^{137}Ba^+$ and eight $^{200}Hg^+$ ions), due to the large spatial separation, sympathetic cooling is highly inefficient. Due to the heat exchange between the two components the decrease of the temperature is very slow. The final temperature for Ba is $\sim$1 K and for Hg$\sim$0.03 K. We are currently investigating in detail the dependence of the efficiency of sympathetic cooling on various parameters and the results will be reported elsewhere.

The rf heating of Coulomb crystals has been investigated by several groups [21,32–34]. In [16] we studied the rf heating of planar crystals: the dependence of the heating rate on the trap parameters and the effects of heating on the structure of the planar crystals. The rf heating of planar bicrystals has not been investigated so far. From our molecular dynamics simulations of rf heating we found out that the ions in the outer shell have larger rf heating rates. This was to be expected as farther from the trap center the rf field is changing more dramatically than near the center. We also expect the ions in the outer shell to heat more when the spatial separation is large because they are pushed farther from the center. This was also confirmed by our simulations. These are illustrated in Fig. 8 in which the rf heating rates of the inner and outer shells for different mass ratios are displayed. Both shells have eight ions of masses M_1 and M_2, respectively. The corresponding bicrystals appear in the insets. For $M_1/M_2=1$ we plotted the rf-heating rate of all 16 ions in the crystal. One can see that the heating rate of the heavy ions (M_2) is larger and that for big mass differences (i.e., large spatial separations) the difference between the rf heating rates of the two components is also large. Figures 7 and 8 show that a large spatial separation, i.e., large mass difference, is not desirable from the point of view of efficient sympathetic cooling or reducing rf heating. The above conclusions are especially relevant for experiments on the sympathetic cooling of molecular ions, organic molecules, or

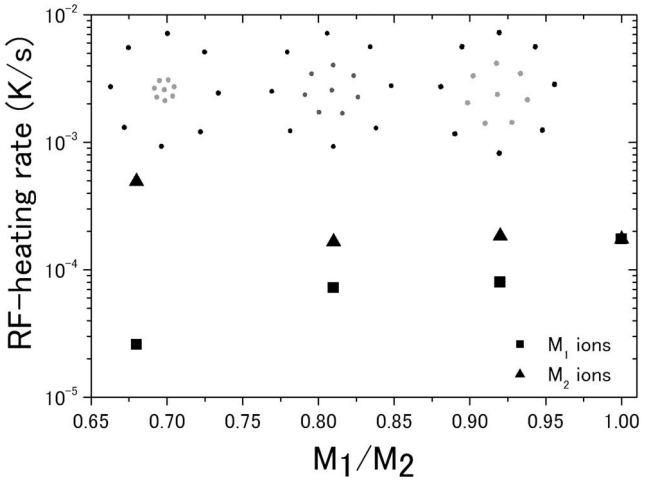

FIG. 8. The rf heating rate of the inner (eight M_1 ions, square) and outer (eight M_2 ions, triangle) shells for different mass ratios. The corresponding bicrystals are also shown. For $M_1/M_2=1$ we plotted the rf heating rate of all 16 ions in the crystal.

heavy highly charged ions. It is important not to forget that in Penning traps the spatial separation has a different cause and therefore Eq. (7) does not apply.

B. Implementing quantum simulation and computation

From the results we presented above it looks like bicrystals composed of isotopes of the same element might be useful for implementing quantum simulation and computation. When the mass difference is small, the inner shell can contain many ions and due to the small radial separation sympathetic cooling is expected to be efficient. Then by continuously cooling the outer shell the inner shell will be maintained cold and therefore it could be used for implementing quantum simulation and computation as proposed in [5]. Let us take the example of a planar bicrystal containing $^{40}Ca^+$ and $^{44}Ca^+$ ions like the ones in Figs. 1 upper) or 3(c) and 3(d). Calcium ions are Doppler cooled using the $S_{1/2}$-$P_{1/2}$ transition (397 nm) and repumping from $D_{3/2}$ to $P_{1/2}$ (866 nm). Selective cooling of only one isotope can be realized using the isotope shifts +842 MHz for $S_{1/2}$-$P_{1/2}$ and −4495 MHz for $D_{3/2}$-$P_{1/2}$. This was demonstrated by our group in [35]. We calculated the rf-heating rate of a planar bicrystal consisting of 20 $^{40}Ca^+$ and 20 $^{44}Ca^+$ with and without continuous cooling of the outer shell. We used the geometric parameters corresponding to the trap in [19] and $U_{ac}=540$ V, $U_z=80$ V. Due to the large U_{ac} we will get large heating rates as shown in [16]. First all cooling is switched off and the kinetic energy is recorded for 50 000 rf periods. The resulting heating rate for $^{40}Ca^+$ is 1.2×10^{-2} K/s and for $^{44}Ca^+$ 1.3×10^{-2} K/s. Next, we do the same thing just this time we let the cooling for $^{44}Ca^+$ stay on. The rf heating is decreased to 4.1×10^{-5} K/s for the inner $^{40}Ca^+$ shell. This numerical example shows the advantage of using planar bicrystals and sympathetic cooling. In experiment, planar bicrystals and multicomponent crystals with arbitrary numbers of ions in each shell could be realized by making use of selective photoionization loading [36] and selective cooling. Continuous cooling of the outer shell would reduce the rf heating of the inner shell significantly and therefore quantum simulation and computation could be implemented in this setup.

VI. CONCLUSIONS

We investigated planar bicrystals in rf traps and found that because of the mass dependence of the radial potential interesting features occur. First, the number of ions in the inner shell is limited by the mass difference between the two components. We calculated the maximum number of ions in the inner shell as a function of the ion masses. Second, the spatial separation between the shells depends on the trapping parameters (i.e., the radial frequency shift) as well as the ion masses and charges. We derived the spatial separation between the shells when strong axial confinement is applied both theoretically and numerically. Then we discussed the effect of spatial separation on sympathetic cooling and rf heating. Finally, we proposed the use of planar bicrystals for implementing quantum computation and simulation by exploiting sympathetic cooling and suggested how this could be realized experimentally.

ACKNOWLEDGMENT

I.M.B. acknowledges the financial support of MEXT.

[1] Y. Masumoto and T. Takagahara, *Semiconductor Quantum Dots: Physics, Spectroscopy and Applications* (Springer-Verlag, Berlin, 2002).
[2] P. Glasson, G. Papageorgiou, K. Harrabi, D. Rees, V. Antonov, E. Collin, P. Fozooni, P. Frayne, Y. Mukharsky, and M. Lea, J. Phys. Chem. Solids **66**, 1539 (2005).
[3] R. Ichiki, Y. Ivanov, M. Wolter, Y. Kawai, and A. Melzer, Phys. Rev. E **70**, 066404 (2004).
[4] B. A. Grzybowski, H. A. Stone, and G. M. Whitesides, Nature (London) **405**, 1033 (2000).
[5] D. Porras and J. I. Cirac, Phys. Rev. Lett. **96**, 250501 (2006).
[6] D. Porras and J. I. Cirac, e-print arXiv:quant-ph/0601148v3.
[7] D. L. Porras and J. I. Cirac, Phys. Rev. Lett. **92**, 207901 (2004).
[8] X. L. Deng, D. Porras, and J. I. Cirac, Phys. Rev. A **72**, 063407 (2005).
[9] D. Porras and J. I. Cirac, Phys. Rev. Lett. **93**, 263602 (2004).
[10] D. Porras, F. Marquardt, J. von Delft, and J. Cirac, Phys. Rev. A **78**, 010101(R) (2008).
[11] J. Taylor and T. Calarco, e-print arXiv:quant-ph/0706.1951.
[12] J. P. Schiffer, Phys. Rev. Lett. **70**, 818 (1993).
[13] M. Block, A. Drakoudis, H. Leuthner, P. Seibert, and G. Werth,

J. Phys. B **33**, L375 (2000).
[14] Y. H. Liu, Z. Y. Chen, M. Y. Yu, L. Wang, and A. Bogaerts, Phys. Rev. E **73**, 047402 (2006).
[15] Y. Liu and L. Chew, J. Phys.: Condens. Matter **19**, 356213 (2007).
[16] I. M. Buluta, M. Kitaoka, S. Georgescu, and S. Hasegawa, Phys. Rev. A **77**, 062320 (2008).
[17] L. Hornekaer, N. Kjaergaard, A. M. Thommesen, and M. Drewsen, Phys. Rev. Lett. **86**, 1994 (2001).
[18] T. Matthey, J. P. Hansen, and M. Drewsen, Phys. Rev. Lett. **91**, 165001 (2003).
[19] A. Mortensen, E. Nielsen, T. Matthey, and M. Drewsen, J. Phys. B **40**, F223 (2007).
[20] F. Major, V. Gheorghe, and G. Werth, *Charged Particle Traps* (Springer-Verlag, Berlia, 2005).
[21] J. Schiffer, J. Phys. B **36**, 511 (2003).
[22] D. H. E. Dubin, Phys. Rev. Lett. **71**, 2753 (1993).
[23] D. Wineland, *Proceeding Cooling, Condensation and Storage of H Cluster Ions Workshop* edited by J. T. Bahns (SRI International, Menlo Park, CA, 1987), p. 181.
[24] T. Matthey, T. Cickovski, S. Hampton, A. Ko, Q. Ma, M. Nyerges, T. Raeder, T. Slabach, and J. Izaguire, ACM Trans. Math. Softw. **30**, 237 (2004).
[25] A. Drakoudis, M. Sollner, and G. Werth, Int. J. Mass. Spectrom. **252**, 61 (2006).
[26] V. M. Bedanov and F. M. Peeters, Phys. Rev. B **49**, 2667 (1994).
[27] T. O'Neil, Phys. Fluids **24**, 1447 (1981).
[28] D. Kielpinski, B. E. King, C. J. Myatt, C. A. Sackett, Q. A. Turchette, W. M. Itano, C. Monroe, D. J. Wineland, and W. H. Zurek, Phys. Rev. A **61**, 032310 (2000).
[29] B. B. Blinov, L. Deslauriers, P. Lee, M. J. Madsen, R. Miller, and C. Monroe, Phys. Rev. A **65**, 040304(R) (2002).
[30] P. Bowe, L. Hornekaer, C. Brodersen, M. Drewsen, J. S. Hangst, and J. P. Schiffer, Phys. Rev. Lett. **82**, 2071 (1999).
[31] T. Baba and I. Waki, Appl. Phys. B: Lasers Opt. **74**, 375 (2002).
[32] C. B. Zhang, D. Offenberg, B. Roth, M. A. Wilson, and S. Schiller, Phys. Rev. A **76**, 012719 (2007).
[33] J. Schiffer, M. Drewsen, J. Hangst, and L. Hronekaer, Proc. Natl. Acad. Sci. U.S.A. **97**, 10697 (2000).
[34] V. L. Ryjkov, X. Z. Zhao, and H. A. Schuessler, Phys. Rev. A **71**, 033414 (2005).
[35] Y. Hashimoto, L. Matsuoka, D. Nagamoto, and S. Hasegawa, Spectrochim. Acta, Part B **63**, 645 (2008).
[36] D. M. Lucas, A. Ramos, J. P. Home, M. J. McDonnell, S. Nakayama, J. P. Stacey, S. C. Webster, D. N. Stacey, and A. M. Steane, Phys. Rev. A **69**, 012711 (2004).